Diez, Ibai, et al. (2017) Enhanced pre-frontal functional-structural networks to support postural control deficits after traumatic brain injury in a pediatric population. *Network Neuroscience*. Advance online publication. doi:10.1162/netn_a_00007.

Enhanced pre-frontal functional-structural networks to support postural control deficits after traumatic brain injury in a pediatric population

Ibai Diez[a], David Drijkoningen[b], Sebastiano Stramaglia[c,d], Paolo Bonifazi[a,g], Daniele Marinazzo[e], Jolien Gooijers [b], Stephan P. Swinnen[b,f,*], Jesus M. Cortes[a,g,h,*]

[a]*Biocruces Health Research Institute, Cruces University Hospital, Barakaldo, Spain.*

[b]*KU Leuven, Movement Control and Neuroplasticity Research Group, Group Biomedical Sciences, Leuven, Belgium.*

[c]*Dipartimento di Fisica, Universita degli Studi di Bari and INFN, Bari, Italy.*

[d]*BCAM - Basque Center for Applied Mathematics, Bilbao, Spain.*

[e]*Department of Data Analysis, Faculty of Psychological and Pedagogical Sciences, University of Ghent, Ghent, Belgium.*

[f]*KU Leuven, Leuven Research Institute for Neuroscience & Disease (LIND), Leuven, Belgium.*

[g]*Ikerbasque: The Basque Foundation for Science, Bilbao, Spain.*

[h]*Department of Cell Biology and Histology, University of the Basque Country, Leioa, Spain.*

**Equal-last author contribution*

Abstract

Traumatic brain injury (TBI) affects the structural connectivity, triggering the re-organization of structural-functional circuits in a manner that remains poorly understood. We focus here on brain networks re-organization in relation to postural control deficits after TBI. We enrolled young participants who had suffered moderate to severe TBI, comparing them to young typically developing control participants. In comparison to control participants, TBI patients (but not controls) recruited prefrontal regions to interact with two separated networks: 1) a subcortical network including part of the motor network, basal ganglia, cerebellum, hippocampus, amygdala, posterior cingulum and precuneus; and 2) a task-positive network, involving regions of the dorsal attention system together with the dorsolateral and ventrolateral prefrontal regions. We also found the increased prefrontal

connectivity in TBI patients was correlated with some postural control indices, such as the amount of body sway, whereby patients with worse balance increased connectivity in frontal regions more strongly. The increased prefrontal connectivity found in TBI patients may provide the structural scaffold for stronger cognitive control of certain behavioural functions, consistent with the observation that various motor tasks are performed less automatically following TBI and that more cognitive control is associated with such actions.

Author Summary

Using a new hierarchical atlas whose modules are relevant for both structure and function, we have found increased structural and functional connectivity in prefrontal regions in TBI patients as compared to controls, in addition to a general pattern of overall decreased connectivity across the TBI brain. Although this increased prefrontal connectivity reflected interactions between brain areas when participants are at rest, the enhanced connectivity was found to be negatively correlated with active behaviour such as the postural control performance. Thus, our findings obtained when the brain is at rest do potentially reflect how TBI patients orchestrate task-related activations to support behaviour in everyday life. In particular, our findings of enhanced connectivity in TBI might help to overcome the deficits in cerebellar and subcortical connections, in addition to compensating for deficits when interacting with the task-positive network. Hence, it appears that there is greater cognitive control over certain actions in order to overcome deficits in their automatic processing.

Keywords: Traumatic Brain Injury, Prefrontal Cortex, Network Reorganization, Resting State, Functional Networks, Structural Networks, Brain Hierarchical Atlas

Diez, Ibai, et al. (2017) Enhanced pre-frontal functional-structural networks to support postural control deficits after traumatic brain injury in a pediatric population. *Network Neuroscience*. Advance online publication. doi:10.1162/netn_a_00007.

1. Introduction

Traumatic brain injury (TBI) involves brain tissue damage as a result of an external mechanical force, such as rapid head acceleration/deceleration or impact. On a neural level, TBI generally disrupts functional and structural large-scale brain networks (ie, the networks of white matter tracts connecting different brain regions), whilst on a behavioural level, TBI often triggers various deficits including cognitive impairments, motor problems, emotional sequelae, etc. even years post-injury (Karen Caeyenberghs et al., 2012; Ham & Sharp, 2012; D. H. Smith & Meaney, 2000). We focus here on deficits in balance control after TBI, which occurring for both adults (Guskiewicz, Riemann, Perrin, & Nashner, 1997; McCulloch, Buxton, Hackney, & Lowers, 2010) and children (Drijkoningen, Caeyenberghs, Vander Linden, et al., 2015; Drijkoningen, Leunissen, et al., 2015; Katz-Leurer, Rotem, Lewitus, Keren, & Meyer, 2008) can last from months to several years after the traumatic impact, which is psychosocially important as it increases the risk of falling and thus affects the patient's independence (McCulloch et al., 2010; Wade, Canning, Fowler, Felmingham, & Baguley, 1997).

Over the past decades imaging techniques such as diffusion weighted imaging (DWI) and functional Magnetic Resonance Imaging (fMRI) have progressed our understanding of the physiopathology of TBI. In particular, recent advances in MRI techniques allowed analysing the injured brain and its correlation with behaviour from a network perspective, i.e., exploring the structural and functional connectivity of neuronal networks in vivo (Barbey et al., 2015; Bonnelle et al., 2011; K. Caeyenberghs et al., 2014; Karen Caeyenberghs et al., 2012; Fagerholm, Hellyer, Scott, Leech, & Sharp, 2015; Ham & Sharp, 2012; Mäki-

Marttunen, Diez, Cortes, Chialvo, & Villarreal, 2013; Sharp et al., 2011; Sharp, Scott, & Leech, 2014). For instance, diffusion weighted results revealed reduced structural connectivity and reduced network efficiency in TBI in relation to poorer cognitive functioning (Bonnelle et al., 2011; K. Caeyenberghs et al., 2014; Fagerholm et al., 2015; Kim et al., 2014) and poorer balance c pediatric ontrol (Karen Caeyenberghs et al., 2012). Moreover, with respect to resting state functional connectivity, i.e., looking at regional BOLD interactions when the brain is at rest, multiple studies have reported TBI-induced alterations (Bonnelle et al., 2011, 2012; F. G. Hillary et al., 2011; Sharp et al., 2011, 2014; Tarapore et al., 2013), even true for cases of mild TBI (Mayer, Mannell, Ling, Gasparovic, & Yeo, 2011; Zhou et al., 2012). It has been shown, for instance, that TBI patients increase functional connectivity within the default mode network (DMN) as compared to healthy controls (F. G. Hillary et al., 2011; Palacios et al., 2013; Sharp et al., 2011), possibly acting as a compensatory mechanism for the loss of structural connections (i.e., axonal injury). Importantly, TBI-induced changes in resting state functional connectivity seem to predict the development of attention impairments (Bonnelle et al., 2011). Finally, the combined information of structural and functional networks resulted in a better prediction of task-switching performance in TBI (Karen Caeyenberghs, Leemans, Leunissen, Michiels, & Swinnen, 2013).

Although there is now sufficient evidence that TBI damages large-scale and emerging properties of brain structural and functional networks, and that the degree of network impairment is correlated with behavioural and cognitive deficits (Drijkoningen, Caeyenberghs, Leunissen, et al., 2015; Palacios et al., 2013; Zhou et al., 2012), the precise pattern of structural-functional circuit re-organization after TBI is still poorly characterized. Here, we use a novel brain atlas (Diez, Bonifazi, et al., 2015) to probe the working

hypothesis that when structural networks are damaged and reorganized as a result of TBI, there is an associated reorganization of the corresponding functional networks, and vice versa, and thus, emphasizing the strong mutual relationship between brain structure and function (Damoiseaux & Greicius, 2009; Diez, Bonifazi, et al., 2015; Park & Friston, 2013). Moreover, in addition to previous work correlating white matter microstructural information with balance performance post-injury (K. Caeyenberghs et al., 2012; Karen Caeyenberghs et al., 2010; Drijkoningen, Caeyenberghs, Leunissen, et al., 2015), we aim here to assess whether this structure-function network reorganization is in any manner related to critical behaviour, such as the postural control deficits after TBI.

2. Materials and Methods

2.1. Participants

The study included a total of 41 young subjects, 14 of whom incurred a TBI (age 13.14 ± 3.25 years; 6 males and 8 females) and 27 healthy control subjects who developed normally (age 15.04 ± 2.26 years; 12 males, 15 females). Group differences for age and sex provided respectively $p = 0.1306$ (after a t-test) and $p = 0.9226$ (after a Chi-squared test), so the TBI and the control groups were age-and-sex matched. TBI patients had suffered moderate to severe head injury, as defined by the Mayo classification system for injury severity. This system classifies patients according to the length of post-traumatic amnesia, loss of consciousness duration, lowest Glasgow Coma Scale score in the first 24 hours, and MRI or computed tomography images, assessed by a specialized clinical neurologist. Demographic data for all patients is given in Table 1. Independently on specific lesions observed during the acute scan (column 2 in Table 2), at the time of the study all 14 TBI patients had diffuse axonal injury, and all of them had no severe focal lesions (column 3 in Table 2). The TBI

patients' mean age at the time of injury was 10 ± 3.45 years, and the average time interval between injury and the present MRI was 3.5 ± 3.5 years. Exclusion criteria were based on pre-existing developmental disorders, central neurological disorders, intellectual disabilities and musculoskeletal disease. Additional exclusion criteria was to have an abbreviated injury score above 2 for upper and lower limbs, thus neglecting serious impaired limb function. The demographic and clinical descriptors of the TBI group are given in Tables 1 and 2.

The study was approved by the Ethics Committee for biomedical research at the KU Leuven and the patients were all recruited from several rehabilitation centres in Belgium (Principal Investigator, Stephan Swinnen). Written informed consent was obtained from either the participants themselves or from the patients' first-degree relatives, according to the Declaration of Helsinki.

2.2 Balance tests

Balance control was assessed using three protocols from the EquiTest System (NeuroCom International, Clackamas, Oregon).

2.2.1 The Sensory Organization Test (SOT):

This test measures static postural control while subjects are standing as still as possible, barefoot, on a movable platform (forceplate) under 4 sensory conditions: 1) eyes open, fixed platform; 2) eyes closed, fixed platform; 3) eyes open with the platform tilting in response to body sway to prevent the ankles from bending (reduced somatosensory feedback); 4) eyes closed, tilting platform. In order to familiarize the subject with the test and to avoid any initial effect of surprise on the sensory manipulations, we included 1 practice trial for each condition prior to completing the actual measurements. After that, each condition was

repeated three times in a randomized order. Each trial lasted twenty seconds. We used an established protocol applied in earlier studies to assess balance control in young and older healthy adults, calculating the centre of pressure (COP) trajectory from the forceplate recordings (100 Hz) (Van Impe, Coxon, Goble, Doumas, & Swinnen, 2012). A mean SOT balance score was acquired for each condition from the 3 trials, excluding trials in which the subject fell. We evaluated the behavioural outcome through the inverse path-length (iPL) of the COP trajectory to acquire a SOT balance index in which higher scores reflect better balance control (and less body sway).

2.2.2 The Limits Of Stability test (LOS):

This is a more dynamic test of balance control that involves goal-directed postural adjustments, where subjects intentionally displace their centre of gravity (COG) in different directions without stepping, falling or lifting their heel or toes. At the beginning of each trial, the COG (provided by the Equitest forceplate) was positioned in the centre, as indicated by a representation on a screen in front of the subject. On presentation of a visual cue and by leaning over in the right direction, the subject had to move the COG from the center towards one of the radial targets presented on the screen as quickly and accurately as possible. The following eight target directions were assessed: front, right front, right, right back, back, left back, left, and left front. After two practice trials, each direction was assessed once in a random order. The trial was interrupted and repeated if the subject fell or took a step, and that trial was not analyzed. Directional control (DC) was computed as the outcome measure reflecting dynamic balance control. Specifically, the DC (expressed as a percentage) was calculated as the difference between on-target (in target direction) and off-target movement (extraneous movement) divided by the amount of on-target movement, as follows: (amount of on-target movement - amount of off-target movement)/(amount of on-target movement) x

100%. Higher scores reflect better DC and only a straight line towards the target would result in a score of 100%, with no off-target movements. Finally, to end up with a single measure to be correlated with imaging results, DC scores were averaged across the eight target directions for further analysis.

2.2.3 The Rhythmic Weight Shift test (RWS):

Like the LOS, this is a dynamic test of balance control measuring the ability to move the COG rhythmically from right to left, or forward and backwards, between two target positions. Each direction (backward-forward, left-right) was performed at 3 different speeds: slow (a pace of 3 seconds between each target), medium (a pace of 2 seconds) and fast (a pace of 1 second). Each combination of speed and direction (a total of 6 combinations) was performed in a separate trial of 6 movement repetitions that were preceded by 4 practice repetitions. The trial was interrupted and repeated if the subject fell or took a step. The DC was calculated as above (similar to LOS) and DC scores were averaged across directions and velocities for further analysis.

In summary, postural control was evaluated through three different score indexes: one measuring static postural control (iPL-SOT), and two measuring dynamical postural control (DC-LOS and DC-RWS). The three indexes were used as behavioural outcome to correlate with imaging results.

2.3 Imaging

2.3.1 MRI acquisition

MRI scanning was performed on a Siemens 3T Magnetom Trio MRI scanner with a 12-channel matrix head coil.

Anatomical data

A high resolution T1 image was acquired with a 3D magnetization prepared rapid acquisition gradient echo (MPRAGE): repetition time [TR] = 2300 ms, echo time [TE] = 2.98 ms, voxel size = 1 × 1 × 1.1mm^3, slice thickness = 1.1 mm, field of view [FOV] = 256 × 240mm^2, 160 contiguous sagittal slices covering the entire brain and brainstem.

Diffusion Tensor Imaging (DTI)

A DTI SE-EPI (diffusion weighted single shot spin-echo echoplanar imaging) sequence was acquired with the following parameters: [TR] = 8000 ms, [TE] = 91 ms, voxel size = 2.2 × 2.2 × 2.2 mm^3, slice thickness = 2.2 mm, [FOV] = 212 × 212 mm^2, 60 contiguous sagittal slices covering the entire brain and brainstem. A diffusion gradient was applied along 64 non-collinear directions with a b value of 1000 s/mm^2. Additionally, one set of images was acquired with no diffusion weighting ($b = 0$ s/mm^2).

Resting state functional data

Resting state fMRI time series were acquired over a 10 minute session using the following parameters: 200 whole-brain gradient echo echoplanar images with [TR/TE] = 3000/30 ms; [FOV] = 230 × 230mm^2; voxel size = 2.5 × 2.5 × 3.1mm^3, 80 × 80 matrix; slice thickness = 2.8 mm; 50 sagittal slices, interleaved in descending order.

2.3.2 MRI pre-processing

Diffusion Tensor Imaging

We applied a DTI preprocessing similar to previous work (Alonso-Montes et al., 2015; Amor et al., 2015; Diez, Bonifazi, et al., 2015) using FSL (FMRIB Software Library v5.0) and the Diffusion Toolkit. First, an eddy current correction was applied to overcome the artefacts produced by variation in the direction of the gradient fields of the MR scanner, together with the artefacts produced by head movements. To ensure that group differences were not due to differences in motion, the average motion of each subject was used as a covariate of non-interest in the statistical analyses. In particular, the motion of the subject in the scanner was extracted from the transformation applied by the eddy current correction step from every volume to the reference volume (the first one, *b=0* volume). Next, using the corrected data, a local fitting of the diffusion tensor was applied to compute the diffusion tensor model for each voxel. Next, a Fiber Assignment by Continuous Tracking (FACT) algorithm was applied (Mori, Crain, Chacko, & van Zijl, 1999). We then computed the transformation from the Montreal Neurological Institute (MNI) space to the individual-subject diffusion space and projected a high resolution functional partition to the latter, composed of 2,514 regions of interest (ROIs), hereon named regions, and generated after applying spatially constrained clustering to the functional data using in (Craddock, James, Holtzheimer, Hu, & Mayberg, 2012). This allowed building 2,514 x 2,514 structural connectivity (SC) matrices, each per subject, by counting the number of white matter streamlines connecting all region pairs within the entire 2,514 regions dataset. Thus, the element matrix (i,j) of SC is given by the streamlines number between regions i and j. SC is a symmetric matrix, where connectivity from i to j is equal to that from j to i. Finally, we made the SC matrices binary for the analysis, considering only two possible values: 0 when

no streamlines existed between i and j; and 1, when any non-zero number existed between the two regions i and j.

Resting state functional MRI

We applied a resting fMRI preprocessing similar to previous work (Alonso-Montes et al., 2015; Amor et al., 2015; Diez, Bonifazi, et al., 2015; Diez, Erramuzpe, et al., 2015; Mäki-Marttunen et al., 2013) by using FSL and AFNI (http://afni.nimh.nih.gov/afni/). First, slice-time correction was applied to the fMRI dataset; next each volume was aligned to the middle volume to correct for head movement artefacts. Next, all voxels were spatially smoothed with a 6 mm full width at half maximum (FWHM) isotropic Gaussian kernel and after intensity normalization, a band pass filter was applied between 0.01 and 0.08 Hz (Cordes et al., 2001) followed by the removal of linear and quadratic trends. We next regressed out the movement time courses, the average cerebrospinal fluid (CSF) signal, the average white-matter signal and the average global signal. Finally, the functional data was spatially normalized to the MNI152 brain template, with a voxel size of 3*3*3 mm^3. In addition to head motion correction, we performed scrubbing, by which time points with framewise displacement bigger than 0.5 were interpolated by a cubic spline (Yan et al., 2013). Further, to remove the effect of head movement in the group comparison analysis, we also used global frame displacement as a covariate of non interest.

2.3.3 Clustering regions of interest into modules by using a new hierarchical brain atlas

The initial 2,514 regions were grouped into modules using a recently published atlas (Diez, Bonifazi, et al., 2015) in which modules are functionally coherent (ie, the dynamics of voxels belonging to one module are very similar) and at the same time, they are structurally wired (ie, the voxels belonging to a given module are interconnected through white matter

fibers). Some existing atlases are purely anatomical or structural (Desikan et al., 2006; Eickhoff et al., 2005; Lancaster et al., 2000; Tzourio-Mazoyer et al., 2002), and others are purely functional, like the one achieved after data driven methods (Craddock et al., 2012). Although obtaining suitable brain partitions (or atlases) has been studied intensively (Craddock et al., 2013), to the best of our knowledge, we were the first to propose a brain partition that accounts for modules that are relevant to both structure and function (Diez, Bonifazi, et al., 2015) which is now implemented in the current project.

Although full details are given in (Diez, Bonifazi, et al., 2015), here, we briefly summarize the hierarchical clustering approach which, applied to a combination of functional and structural datasets, resulted in a hierarchical tree or dendrogram in which nodes were progressively merged together into M different moduli following a nested hierarchy of "similarity" (which reflects correlation for the functional data and white matter streamlines-number for the structural one). Thus, cutting the tree at a certain level led to a pooling of the initial 2,514 ROIs into a finite number of modules $1 \leq M \leq 2{,}514$ (in principle, an arbitrary number for M can be obtained by varying the depth of the cut). Thus, to provide some examples, the highest dendrogram level *M=1* corresponded to all 2,514 regions belonging to a single module, coincident with the entire brain, whereas the lowest level *M=2,514* corresponded to 2,514 separated modules, all of them composed of one single region.

It was also shown in (Diez, Bonifazi, et al., 2015) that the hierarchical brain partition with *M=20* modules was optimal based on cross-modularity, an index simultaneously accounting for three features: 1) Modularity of the structural partition; 2) Modularity of the functional partition; and 3) Similarity between functional and structural modules. The matlab code to

calculate the cross-modality index between structural and functional connectivity matrices can be downloaded at http://www.nitrc.org/projects/biocr_hcatlas/

To compute cross-modularity, we first assessed modularity simply for accounting the quality of the brain partition, i.e., a partition with high modularity has modules highly isolated from each other, achieved for instance by maximizing the fraction of intra-module to inter-module connections with respect to randomizations. In particular, we applied the Newman's algorithm to address modularity (Newman, 2004). In addition to modularity, cross-modularity made use of the similarity between structural and functional modules, which was approached by calculating the Sorensen's index, a normalized quantity equal to twice the number of common connections in the two modules divided by the total number of connections in the two modules.

The entire hierarchical brain partition can be downloaded at http://www.nitrc.org/projects/biocr_hcatlas/

2.4 Statistical analyses

2.4.1 Behavioural data

Balance control scores iPL-SOT, DC-LOS and DC-RWS were compared between TBI and Healthy Control groups by using a two tailed t-test.

2.4.2 Imaging data

Group differences in structural networks

From the modules defined in the hierarchical atlas, structural networks (SN) were assessed by counting all the connections (ie, streamlines) starting from one module and ending in a

different one. Notice that modules can be defined at any level of the hierarchical tree. We then calculated the module's connectivity degree (the total number of connections reaching a module which coincides with the total number of connections leaving it, as the structural connectivity is a symmetric matrix).

Next, we applied a two-sample t-test using age and average head motion as covariate of non-interest to search for significant differences ($p< 0.05$). In particular, to test if the means of two groups differed, we performed the hypothesis test using a general linear model, where Y contains the data and X the experimental design variables and confounds. Using the appropriate contrast (searching for mean group differences whilst removing the confound variables), we computed a two sample unpaired t-test.

To assess the significance of the structural differences, we applied a permutation test by performing 1,000 random subject label permutations. We then generated the probability distribution for these values, which constitutes the null-hypothesis since all the dependencies have been removed by the shuffling procedure. All regions with $p > 0.05$ were discarded.

A final remark, although the original SC matrices of size 2,514*2,514 were binarized, however, at the moduli level we worked with weighted degrees for the group comparison analysis.

Group differences in resting state brain dynamics within individual regions

In order to determine group differences in the resting state brain dynamics within each of the $M=20$ modules, we first obtained the time-series of the first principal component for each module, chosen as a representative for the entire module. Next, we compared 4 different descriptors extracted from these time series: variance (2^{nd} standardized moment; quantifies

fluctuation size), skewness (3rd standardized moment; identifies extreme brain dynamics in the resting state (Amor et al., 2015) as it measures how much asymmetry a distribution has with respect to its mean), kurtosis (4th standardized moment; measures the long-tail effect on the data distribution), and the number of points resulting from the point process analysis (PPA, measured by counting the number of amplitude peaks in the BOLD signal (Tagliazucchi, Balenzuela, Fraiman, & Chialvo, 2012), and in particular, counting the points with value greater than the mean value of the time series plus 1 SD). These descriptors were subjected to a two-sample t-test with age and head motion as covariates to evaluate the differences between the TBI and control participants (p <0.05).

Group differences in functional networks

Motivated by an earlier study (S. M. Smith et al., 2009), functional networks (FN) were assessed by quantifying the interaction between each of the *M=20* modules and the rest of the brain (figure S1). First, within each of the *M=20* modules, we applied a principal component analysis (PCA) to reduce the dimension of the data, resulting in 20 components for each of the *M=20* modules. Next, we applied an independent component analysis (ICA) to obtain *C=20* independent time-series components associated to each of the *M=20* modules. Finally, we applied a general lineal model to quantify the contribution of each brain voxel to each component (i.e., component's spatial map). Next, we clustered all spatial maps by applying the k-means clustering-algorithm using the spatial correlation between observations as the similarity measure (Bishop, 2006); thus, two maps belonged to the same cluster if they showed high spatial correlation. After k-means, the 820 observations per module (41 subjects, *C=20* independent components) were grouped into 5 clusters, that we named the 5 most representative clusters (MRCs). Here, the number 5 was chosen by careful inspection to guarantee a good discrimination between the different clusters. K-means, in

addition to returning the 5 MRCs, also provided one label for each of the 820 observations, 1,2,3,4 or 5, indicating to which MRC the observation belongs.

As a result of PCA+ICA we obtained 20 spatial maps per module and subject. Each spatial map, i.e., an observation, was assigned to one of the 5 MRCs, and this occurred for each module. We took all the spatial maps, per MRC and module, and performed a t-test comparing between TBI and healthy controls.

For multiple comparison correction due to a voxel-by-voxel analysis, a statistical significant cluster-level Family Wise Error (FWE) was applied. In particular, a Monte-Carlo simulation (3dClustSim, AFNI, http://afni.nimh.nih.gov) was performed with 10,000 iterations to estimate the probability of false positive clusters with $p<0.05$, corrected with FWE. We used the new version of the software, which corrects for the bug detected in (Eklund, Nichols, & Knutsson, 2016). After correcting for multiple comparisons, three classes of activity maps for each region were calculated: 1) the average FN in control participants (corresponding to the contrast [1 0 0 0], the last two zeros correspond to movement and age variables); 2) the average FN in TBI (contrast [0 1 0 0]); and 3) the differences in average FN between control and TBI (applying the two different contrasts [1 -1 0 0] and [-1 1 0 0] we achieve, respectively, control > TBI connectivity and TBI > control connectivity).

Important to note is that all TBI patients at the MRI session used in this study had diffuse axonal injury, with no severe focal lesions or regional atrophy, which justifies the pooling of all TBI patients into the same group to be compared with a group of healthy controls.

2.4.3 Relationship between behavioural and imaging data

We used a general linear model using the age and average frame displacement as covariate of non-interest to estimate the relationship between postural control and the variance/kurtosis/skewness/PPA in every voxel. Next, we used a t-test to assess the association between the postural control scores (iPL-SOT, DC-LOS and DC-RWS) and the different fMRI measures, using 3dClustSim with a cluster-based FWE multiple comparisons correction. Within this region, we used the mask of TBI>control structural connectivity and correlated the variance/kurtosis/skewness/PPA of voxels within this region with the three behavioural scores. To assess the association between the postural control variable and the fMRI variables, we took the region that survive for multiple comparisons and plotted the correlation of the *corrected* variance (i.e., the variance after removing the effect of age and head motion) and the postural control variable. We performed both Pearson and Spearman correlational analyses, the latter being less affected by the presence of outliers.

3. Results

3.1 TBI-induced alterations in postural control performance

Alterations in postural control performance were measured by three different tests (ie, SOT, LOS, RWS). First, the Sensory Organization Test showed that TBI patients had a smaller inverse path-length in the COP trajectory as compared to control participants (iPL-SOT, control: 106.72 +- 8.41; TBI: 88.63 +- 28.80; *p=0.0041*; *t=3.054*), which reflects that TBI patients had a worse balance (more body sway) than control. Similarly, the Rhythmic Weight Shift test showed that TBI patients performed poorer as compared to controls (DC-RWS, control: 83.77 +- 7.01; TBI: 77.11 +- 9.82; *p=0.0174*; *t=2.4868*), confirming a poorer dynamic balance for TBI patients. In contrast, the limits of stability test did not show group

significant differences as measured by the dynamic control index (DC-LOS, control: 83.80 +- 6.75; TBI: 83.46 +- 5.89; *p=0.8731*; *t=0.1608*).

3.2. TBI-induced alterations in structural networks

Alterations in structural networks were assessed by calculating the connectivity degree for each module in the hierarchical atlas from the inter-module connectivity matrix and performing a group comparison (after correcting for multiple comparisons by performing random subject label permutations). At the level of *M=20* modules (Table 3), control participants showed a higher number of connections reaching another module as compared to TBI patients (figure 1). This suggests a global decrease in connectivity associated with TBI. More specifically, significant differences in connectivity degree were evident within module 14 (*p=0.01*, *t=2.64*), a module including part of the hippocampus and parahippocampal gyrus, amygdala, putamen, insula, ventral diencephalon, temporal gyrus and temporal pole) and module 20 (*p=0.003*, *t=3.13*), a module including part of the cerebellum and parahippocampal gyrus). See Table 4 for full statistical details.

At the level of *M=20* in the hierarchical tree the inter-module connectivity degree was higher in controls relative to patients, indicating that one needs to go down on the hierarchical tree to find another representation with a higher spatial scale where TBI connectivity might be higher as compared to control connectivity (the number of *M* modules decreases as the tree goes down). Proceeding in this way, at the level of *M=120* modules we found higher connectivity values for TBI patients relative to controls within module 11 of the hierarchical atlas (*p=0.009*, *t=2.75*). This module includes part of the caudate nucleus, nucleus accumbens, lateral frontal orbital gyrus, orbital gyrus and anterior cingulate gyrus. Thus, whilst at the level of *M=20* TBI reduced connectivity as compared to controls, at the

level of *M=120* modules (ie, at a higher spatial scale) prefrontal regions showed an increase in connectivity for TBI as compared to controls.

3.3 TBI-induced alterations in resting state brain dynamics within individual modules

Alterations in the resting state brain dynamics within each of the *M=20* modules were assessed by calculating the differences in the time series of the first principal component extracted from each module (figure 2). Explained data variance across modules varied from 28% to 54%, with a mean value of 38%. In particular, differences were addressed with respect to the second moment (ie, *variance*), the third moment (*skewness*), the forth moment (*kurtosis*) and the number of time-series points that had a value above the mean value of the time series plus 1 times the standard deviation. After repeating the same procedure for all *M=20* modules of the hierarchical atlas, significant differences were only present within module 11 (*p=0.01*, *t=-2.55*, explained data variance of the first principal component equal to 48.55%), revealing that brain dynamics variance was higher in the TBI than in the control group. Full statistical details are given in Table 5.

3.4 TBI-induced alterations in functional networks

Functional networks were addressed by quantifying the interaction from each of the *M*=20 modules to the rest of the brain. Within each module, we first obtained *C=20* components (after PCA followed by ICA) and next, we performed spatial regression of the *C=20* components to all the brain voxels, in this way obtaining *C=20* spatial maps for each of the modules. We grouped all the 820 observations (41 subjects, *C=20* independent components) per each module into the 5 most representative clusters (MRCs).

After this procedure, it was possible to obtain the same MRC from different modules. In particular, figure 3 shows the results associated to one of the MRCs obtained from the following modules: module 3 (including part of the sensory-motor and auditory networks), modules 14 and 15 (including part of the thalamus, hippocampus, amygdala, putamen, ventral diencephalon and insula), module 18 (including part of the hippocampus and entorhinal cortex, fusiform gyrus, inferior and middle temporal gyrus and parahippocampal gyrus), module 19 (including part of the cerebellum and brainstem) and module 20 (including part of the cerebellum and parahippocampal gyrus).

The anatomical representation of this MRC (obtained from modules 3, 14, 15, 18, 19 and 20) revealed a *subcortical network* (see figure 3 - columns “FN in control” and “FN in TBI”), consisting of part of the motor network, basal ganglia, cerebellum, thalamus, parahippocampus, hippocampus, precuneus, amygdala, insula, caudate nucleus, putamen and pallidum. Interestingly, the TBI > control connectivity comparison (obtained with the contrast [-1 1 0 0]) revealed one cluster in the frontal lobe (figure 3 – column “differences”, colored in blue), a region including part of the middle frontal and superior orbital gyrus, rectus, olfactory lobe, frontal medial orbital, precuneus and cingulum anterior. In other words, the subcortical network illustrated in figure 3 with labels "FN in control" and "FN in TBI" recruited the prefrontal brain in TBI patients but did not happen for control participants.

A different MRC resembled the *task-positive network* (figure 4 - columns “FN in control” and “FN in TBI”). In particular, this MRC consisted of parts of the cerebellum, lingual gyrus, fusiform gyrus, inferior occipital gyrus, calcarine sulcus, cuneus, precuneus, superior temporal pole, superior motor area and insula. The MRC resulted from the functional interactions with module 1 (including part of the posterior cingulate gyrus), module 4 (the medial visual network), module 5 (including part of the medial frontal gyrus, precentral

gyrus and rostral pars of the middle frontal gyrus), module 12 (including part of the inferior parietal gyrus, inferior temporal gyrus, lateral frontal orbital gyrus, pars orbitalis, pars triangularis, rostral pars of the middle frontal gyrus, superior frontal gyrus, caudate nucleus and anterior cingulate gyrus), and modules 14 and 15 (including part of the thalamus, hippocampus, amygdala, putamen, ventral diencephalon and insula).

Although both control and TBI groups revealed a similar task-positive network (figure 4 - columns “FN in control” and “FN in TBI”), the connectivity in TBI > control connectivity contrast (figure 4 – column “differences”, colored in blue) revealed a network in the frontal brain, more specifically a network including part of the frontal medial orbital, anterior cingulum, precuneus, superior frontal and angular gyrus. Thus, similar to the subcortical network represented in figure 3, the task-positive network recruited the prefrontal cortex in TBI patients but did not for control participants.

3.5 Brain regions showing increased connectivity in TBI for both functional and structural networks

Since we observed an increased connectivity in TBI patients relative to controls for both functional and structural networks, we decided to take a closer look at these overlapping findings by superimposing these regions (figure 5). With regard to the analysis performed for structural networks, a higher connectivity degree in TBI was found in a small subnetwork, composed by a hub (figure 5a - plotted in red) connecting to other regions (figure 5a - areas in green). The region's hub belongs to module 11 of the hierarchical atlas and connects to superior frontal regions, anterior cingulum, thalamus, striatum, insula, amygdala, hippocampus and parahippocampus, olfactory lobe and cerebellum.

With regard to the analysis performed for functional networks (figure 5b), two regions showed increased connectivity in TBI as compared to controls: one region interacting with a subcortical network (including superior frontal gyrus, superior medial frontal gyrus and middle frontal gyrus, and anterior cingulum) and another region interacting with the task-positive network (including anterior cingulum, frontal medial gyrus, middle orbital gyrus superior frontal medial gyrus and rectus).

By looking at both figures 5a and 5b, there exists an overlap between the map of increased structural connectivity (figure 5a) and the maps corresponding to increased functional connectivity (figure 5b), and this occurred, for both the subcortical and the task-positive networks.

3.6 Relation between postural control and prefrontal dynamics at rest

We found that within module 11 of the hierarchical atlas there was an increase in connectivity for both structural and functional networks for TBI patients when compared to control participants. Correlational analyses revealed that the prefrontal dynamics activation at rest of module 11 (represented by the *corrected* variance of the voxel fMRI dynamics), was correlated to the inverse path-length score of the static SOT test (iPL-SOT), giving a Pearson correlation of $r=-0.86$ ($p=0.00013$) and a Spearman correlation of $s=-0.78$ ($p=0.0026$). These results suggest that a better balance performance is associated with decreased dynamical activation in region 11. Neither DC-RWS nor DC-LOS were significant correlated to any of the fMRI measures within module 11.

4. Discussion

Here, we provide the first evidence that TBI-induced alterations in functional and structural networks show overlapping results. With respect to both neuronal networks TBI patients demonstrate as compared with controls increased prefrontal connectivity. Moreover, these TBI-induced network alterations are associated with changes in balance performance.

TBI-induced alterations in structural networks. In agreement with previous studies (Gentry, Godersky, & Thompson, 1988; Hulkower, Poliak, Rosenbaum, Zimmerman, & Lipton, 2013; Zappalà, Thiebaut de Schotten, & Eslinger, 2012), we found that TBI patients showed reduced structural connectivity (i.e., smaller connectivity degree) for most brain areas compared to healthy participants. More precisely, we found a strong decrease in connectivity degree in motor areas, brainstem, cingulum, cerebellum and temporal poles, areas that are typically associated with the performance of motor skills and balance control. Indeed, decreased subcortical connectivity, in particular in the brainstem and cerebellum, was recently associated with postural impairments in TBI patients (Drijkoningen, Leunissen, et al., 2015), suggesting a possible diffuse pathology across subcortical structures.

Although for most brain areas we found a lower connectivity degree in TBI relative to controls, we also found a higher connectivity degree in TBI relative to controls exclusively in the prefrontal cortex. This finding, together with the observation that TBI patients have a poorer performance in postural control, may provide a mechanism for stronger cognitive control of such motor actions.

TBI-induced alterations in functional networks. Our approach, focusing on interactions between modules defined by the hierarchical atlas at rest, revealed that TBI patients incorporated the prefrontal cortex together with a subcortical network. This possibly suggests a mechanism compensating for TBI-induced subcortical-cortical axonal disruptions,

as confirmed by the results found in the analysis of structural networks, showing decreased white matter connectivity in cortical to subcortical pathways. This disconnection is also consistent with grey matter deficits reported in the frontal and temporal cortices, cingulate gyrus, as well as within subcortical structures, including the cerebellum (Gale, Baxter, Roundy, & Johnson, 2005; Zappalà et al., 2012).

We also found that TBI patients incorporated the prefrontal cortex to the task-positive network (Fox et al., 2005), employed during performance of attention-demanding tasks. This suggests more cognitive control and less automatic movement in TBI patients than in control participants.

TBI-induced alterations in both structural and functional networks and association with behaviour. In many studies of brain networks, changes in functional or in structural network connectivity have often been associated with TBI, yet very few studies have addressed their combination. Here, we have shown that prefrontal brain areas in TBI patients increase structural and functional connectivity as compared to control participants, and the resting dynamics of the areas where connectivity increases is negatively correlated to postural control performance. This may refer to a compensatory *plasticity* mechanism that suggests a different mode of balance control, namely, increased controlled processing or less automatic processing of balance movements. Thus, it is not a successful compensation whereby increased functional and structural connectivities lead to increased balance performance but, rather, a mandatory change in performance mode to be able to accomplish the balance tasks.

Previous work found prefrontal increased functional connectivity in patients after TBI (Gooijers et al., 2016; Frank G. Hillary, Genova, Chiaravalloti, Rypma, & DeLuca, 2006;

Rasmussen et al., 2008); but, as far as we know, we provide for the first time evidence that when structural networks are damaged as a result of brain pathology, an associated reorganization of the corresponding functional networks is also established, and vice versa. Moreover, the prefrontal cortex is the most appropriate locus from where this network reorganization is orchestrated.

It is well known that prefrontal areas do not operate in isolation. In particular, it has been widely reported that interactions between the frontal cortex and the basal ganglia play a key role in movement control (Alexander, Crutcher, & DeLong, 1990; Aron, 2006; Coxon et al., 2010; Coxon, Van Impe, Wenderoth, & Swinnen, 2012; Hikosaka & Isoda, 2010; Mink, 1996). Thus, the fronto-striato-thalamic circuit, which enables frontal lobe regions to communicate with the basal ganglia, is involved in a rich spectrum of different functions: motor and oculomotor circuits, executive functions, social behaviour and motivational states, see for instance (Frank, Scheres, & Sherman, 2007). Moreover, there is evidence that the reported reduced connectivity in the fronto-striato-thalamic circuit we found is correlated with a reduced subcortical grey matter volume and task performance after TBI (Leunissen et al., 2014a, 2014b).

Furthermore, it has been shown that white matter connectivity and subcortical gray matter volume continue to decrease up to 4 years post-injury (Eierud et al., 2014; Farbota et al., 2012), which may lead to a reorganization of the prefrontal brain regions to compensate for the damage to the fronto-striato-thalamic circuit. This potential response to the insult is in agreement with our findings and previous results (Leunissen et al., 2014a, 2014b; Palacios et al., 2013).

Methodological issues and current limitations

We are aware that the clinical population we are studying is small (*N=14*) and highly heterogeneous, with time since injury varying from 4 months to 10 years and age range varying from 8 to 19 years. However, patients with moderate to severe TBI in a pediatric population are challenging to recruit. While we recruited additional patients, these patients had focal brain lesions, and thus their inclusion in our sample would have further increased sample heterogeneity. This motivated us to limit our cohort to *N=14* patients, all with diffuse brain injury. Future work, involving larger subject cohorts and/or more homogeneous samples, is needed to fully address these limitations.

Functional connectivity matrices depend crucially on the specific steps used in the pre-processing pipelines. One step that affects severely connectivity matrices is the subtraction (or not) of the global signal regression. Here, in agreement with previous work (Alonso-Montes et al., 2015; Amor et al., 2015; Diez, Bonifazi, et al., 2015; Diez, Erramuzpe, et al., 2015; Mäki-Marttunen et al., 2013; Marinazzo et al., 2014; S. Stramaglia, Angelini, Cortes, & Marinazzo, 2015; Sebastiano Stramaglia et al., 2016), we subtracted to each individual time series the global signal regression that is well-known to add negative correlations into the functional connectivity matrices (Murphy, Birn, Handwerker, Jones, & Bandettini, 2009; Saad et al., 2012). After repeating the entire analysis without subtracting the global signal regression, figure 3 did not change, but the results shown in 4 were different. In particular, the significance of the prefrontal regions interacting with the task-positive network did not preserve after multiple comparisons (but did exist for uncorrected multiple comparisons).

To perform group comparison between the SC matrices, we assessed differences in module degree statistics, which allows localizing brain regions *connected* differently in the two groups, but beyond node-degree group differences, there exist alternative network statistics (based on measures that go more deep into the network topology) for identifying group

differences (Zalesky, Fornito, & Bullmore, 2010). Future work will take this into consideration.

Recent work has suggested that tractography algorithms might produce false positive connectivity increases in the pathology of TBI (Squarcina, Bertoldo, Ham, Heckemann, & Sharp, 2012), mainly due to the existence of smaller FA values in different tracts after TBI, which ultimately might translate into an inaccurate tractography (i.e., counting more streamlines than they really exist). We performed group comparison (FWE, 3dClustSim) between FA values between control and TBI and found that FA values in the prefrontal brain areas were not significant smaller in TBI as compared to controls (results not shown), thus corroborating that the increased connectivity found in TBI as compared to control in this work is not a consequence of this issue.

The main motivation to use the brain hierarchical atlas is that the different modules are meaningful for both structure and function. The analysis based on the PCA+ICA post-processing (figure S1), only used for figures 3 and 4, is not specific to the atlas per se but a functional strategy to extract information beyond the average activity within a region (i.e. the first principal component). Therefore, this strategy is in general valid for any other brain partition.

Acknowledgments

ID undertook a 2 month lab rotation to visit the laboratories of Swinnen and Marinazzo that was funded by the Health Department of the Basque Goverment. SS acknowledges financial support from Bizkaia Talent and European Commission through COFUND with the research project BRAhMS – Brain Aura Mathematical Simulation– (AYD-000-285). JMC

acknowledges financial support from Ikerbasque: The Basque Foundation for Science, grant DPI2016-79874-R from Ministerio Economia, Industria y Competitividad (Spain) and FEDER and Euskampus at UPV/EHU. SPS was supported by FWO Vlaanderen (Levenslijn G.A114.11 and G.0708.14), the Research Fund KU Leuven (C16/15/070) and the Interuniversity Attraction Poles program of the Belgian federal government (Belspo, P7/11).

References:

Alexander, G. E., Crutcher, M. D., & DeLong, M. R. (1990). Basal ganglia-thalamocortical circuits: parallel substrates for motor, oculomotor, “prefrontal” and “limbic” functions. *Progress in Brain Research*, *85*, 119–146.

Alonso-Montes, C., Diez, I., Remaki, L., Escudero, I., Mateos, B., Rosseel, Y., … Cortes, J. M. (2015). Lagged and instantaneous dynamical influences related to brain structural connectivity. *Frontiers in Psychology*, *6*, 1024. https://doi.org/10.3389/fpsyg.2015.01024

Amor, T. A., Russo, R., Diez, I., Bharath, P., Zirovich, M., Stramaglia, S., … Chialvo, D. R. (2015). Extreme brain events: Higher-order statistics of brain resting activity and its relation with structural connectivity. *EPL (Europhysics Letters)*, *111*(6), 68007. https://doi.org/10.1209/0295-5075/111/68007

Aron, A. R. (2006). Cortical and Subcortical Contributions to Stop Signal Response Inhibition: Role of the Subthalamic Nucleus. *Journal of Neuroscience*, *26*(9), 2424–2433. https://doi.org/10.1523/JNEUROSCI.4682-05.2006

Barbey, A. K., Belli, A., Logan, A., Rubin, R., Zamroziewicz, M., & Operskalski, J. T. (2015). Network topology and dynamics in traumatic brain injury. *Current Opinion in Behavioral Sciences*, *4*, 92–102. https://doi.org/10.1016/j.cobeha.2015.04.002

Bishop, C. M. (2006). *Pattern recognition and machine learning*. New York: Springer.

Bonnelle, V., Ham, T. E., Leech, R., Kinnunen, K. M., Mehta, M. A., Greenwood, R. J., & Sharp, D. J. (2012). Salience network integrity predicts default mode network function after traumatic brain injury. *Proceedings of the National Academy of Sciences of the United States of America*, *109*(12), 4690–4695. https://doi.org/10.1073/pnas.1113455109

Bonnelle, V., Leech, R., Kinnunen, K. M., Ham, T. E., Beckmann, C. F., De Boissezon, X., … Sharp, D. J. (2011). Default mode network connectivity predicts sustained attention deficits after traumatic brain injury. *The Journal of Neuroscience: The Official Journal of the Society for Neuroscience*, *31*(38), 13442–13451. https://doi.org/10.1523/JNEUROSCI.1163-11.2011

Caeyenberghs, K., Leemans, A., De Decker, C., Heitger, M., Drijkoningen, D., Linden, C. V., … Swinnen, S. P. (2012). Brain connectivity and postural control in young traumatic brain injury patients: A diffusion MRI based network analysis. *NeuroImage: Clinical*, *1*(1), 106–115. https://doi.org/10.1016/j.nicl.2012.09.011

Caeyenberghs, K., Leemans, A., Geurts, M., Taymans, T., Linden, C. V., Smits-Engelsman, B. C. M., … Swinnen, S. P. (2010). Brain-behavior relationships in young traumatic brain injury patients: DTI metrics are highly correlated with postural control. *Human Brain Mapping*, *31*(7), 992–1002. https://doi.org/10.1002/hbm.20911

Caeyenberghs, K., Leemans, A., Heitger, M. H., Leunissen, I., Dhollander, T., Sunaert, S., … Swinnen, S. P. (2012). Graph analysis of functional brain networks for cognitive control of action in traumatic brain injury. *Brain: A Journal of Neurology*, *135*(Pt 4), 1293–1307. https://doi.org/10.1093/brain/aws048

Caeyenberghs, K., Leemans, A., Leunissen, I., Gooijers, J., Michiels, K., Sunaert, S., & Swinnen, S. P. (2014). Altered structural networks and executive deficits in

traumatic brain injury patients. *Brain Structure & Function*, *219*(1), 193–209. https://doi.org/10.1007/s00429-012-0494-2

Caeyenberghs, K., Leemans, A., Leunissen, I., Michiels, K., & Swinnen, S. P. (2013). Topological correlations of structural and functional networks in patients with traumatic brain injury. *Frontiers in Human Neuroscience*, *7*, 726. https://doi.org/10.3389/fnhum.2013.00726

Cordes, D., Haughton, V. M., Arfanakis, K., Carew, J. D., Turski, P. A., Moritz, C. H., … Meyerand, M. E. (2001). Frequencies contributing to functional connectivity in the cerebral cortex in "resting-state" data. *AJNR. American Journal of Neuroradiology*, *22*(7), 1326–1333.

Coxon, J. P., Goble, D. J., Van Impe, A., De Vos, J., Wenderoth, N., & Swinnen, S. P. (2010). Reduced basal ganglia function when elderly switch between coordinated movement patterns. *Cerebral Cortex (New York, N.Y.: 1991)*, *20*(10), 2368–2379. https://doi.org/10.1093/cercor/bhp306

Coxon, J. P., Van Impe, A., Wenderoth, N., & Swinnen, S. P. (2012). Aging and inhibitory control of action: cortico-subthalamic connection strength predicts stopping performance. *The Journal of Neuroscience: The Official Journal of the Society for Neuroscience*, *32*(24), 8401–8412. https://doi.org/10.1523/JNEUROSCI.6360-11.2012

Craddock, R. C., James, G. A., Holtzheimer, P. E., Hu, X. P., & Mayberg, H. S. (2012). A whole brain fMRI atlas generated via spatially constrained spectral clustering. *Human Brain Mapping*, *33*(8), 1914–1928. https://doi.org/10.1002/hbm.21333

Craddock, R. C., Jbabdi, S., Yan, C.-G., Vogelstein, J. T., Castellanos, F. X., Di Martino, A., … Milham, M. P. (2013). Imaging human connectomes at the macroscale. *Nature Methods*, *10*(6), 524–539. https://doi.org/10.1038/nmeth.2482

Damoiseaux, J. S., & Greicius, M. D. (2009). Greater than the sum of its parts: a review of studies combining structural connectivity and resting-state functional connectivity. *Brain Structure & Function*, *213*(6), 525–533. https://doi.org/10.1007/s00429-009-0208-6

Desikan, R. S., Ségonne, F., Fischl, B., Quinn, B. T., Dickerson, B. C., Blacker, D., … Killiany, R. J. (2006). An automated labeling system for subdividing the human cerebral cortex on MRI scans into gyral based regions of interest. *NeuroImage*, *31*(3), 968–980. https://doi.org/10.1016/j.neuroimage.2006.01.021

Diez, I., Bonifazi, P., Escudero, I., Mateos, B., Muñoz, M. A., Stramaglia, S., & Cortes, J. M. (2015). A novel brain partition highlights the modular skeleton shared by structure and function. *Scientific Reports*, *5*, 10532. https://doi.org/10.1038/srep10532

Diez, I., Erramuzpe, A., Escudero, I., Mateos, B., Cabrera, A., Marinazzo, D., … Alzheimer's Disease Neuroimaging Initiative. (2015). Information Flow Between Resting-State Networks. *Brain Connectivity*, *5*(9), 554–564. https://doi.org/10.1089/brain.2014.0337

Drijkoningen, D., Caeyenberghs, K., Leunissen, I., Vander Linden, C., Leemans, A., Sunaert, S., … Swinnen, S. P. (2015). Training-induced improvements in postural control are accompanied by alterations in cerebellar white matter in brain injured patients. *NeuroImage. Clinical*, *7*, 240–251. https://doi.org/10.1016/j.nicl.2014.12.006

Drijkoningen, D., Caeyenberghs, K., Vander Linden, C., Van Herpe, K., Duysens, J., & Swinnen, S. P. (2015). Associations between Muscle Strength Asymmetry and Impairments in Gait and Posture in Young Brain-Injured Patients. *Journal of Neurotrauma*, *32*(17), 1324–1332. https://doi.org/10.1089/neu.2014.3787

Drijkoningen, D., Leunissen, I., Caeyenberghs, K., Hoogkamer, W., Sunaert, S., Duysens, J., & Swinnen, S. P. (2015). Regional volumes in brain stem and cerebellum are

associated with postural impairments in young brain-injured patients. *Human Brain Mapping*, *36*(12), 4897–4909. https://doi.org/10.1002/hbm.22958

Eickhoff, S. B., Stephan, K. E., Mohlberg, H., Grefkes, C., Fink, G. R., Amunts, K., & Zilles, K. (2005). A new SPM toolbox for combining probabilistic cytoarchitectonic maps and functional imaging data. *NeuroImage*, *25*(4), 1325–1335. https://doi.org/10.1016/j.neuroimage.2004.12.034

Eierud, C., Craddock, R. C., Fletcher, S., Aulakh, M., King-Casas, B., Kuehl, D., & LaConte, S. M. (2014). Neuroimaging after mild traumatic brain injury: review and meta-analysis. *NeuroImage. Clinical*, *4*, 283–294. https://doi.org/10.1016/j.nicl.2013.12.009

Eklund, A., Nichols, T. E., & Knutsson, H. (2016). Cluster failure: Why fMRI inferences for spatial extent have inflated false-positive rates. *Proceedings of the National Academy of Sciences*, *113*(28), 7900–7905. https://doi.org/10.1073/pnas.1602413113

Fagerholm, E. D., Hellyer, P. J., Scott, G., Leech, R., & Sharp, D. J. (2015). Disconnection of network hubs and cognitive impairment after traumatic brain injury. *Brain: A Journal of Neurology*, *138*(Pt 6), 1696–1709. https://doi.org/10.1093/brain/awv075

Farbota, K. D. M., Sodhi, A., Bendlin, B. B., McLaren, D. G., Xu, G., Rowley, H. A., & Johnson, S. C. (2012). Longitudinal volumetric changes following traumatic brain injury: a tensor-based morphometry study. *Journal of the International Neuropsychological Society: JINS*, *18*(6), 1006–1018. https://doi.org/10.1017/S1355617712000835

Fox, M. D., Snyder, A. Z., Vincent, J. L., Corbetta, M., Van Essen, D. C., & Raichle, M. E. (2005). From The Cover: The human brain is intrinsically organized into dynamic, anticorrelated functional networks. *Proceedings of the National Academy of Sciences*, *102*(27), 9673–9678. https://doi.org/10.1073/pnas.0504136102

Frank, M. J., Scheres, A., & Sherman, S. J. (2007). Understanding decision-making deficits in neurological conditions: insights from models of natural action selection. *Philosophical Transactions of the Royal Society B: Biological Sciences*, *362*(1485), 1641–1654. https://doi.org/10.1098/rstb.2007.2058

Gale, S. D., Baxter, L., Roundy, N., & Johnson, S. C. (2005). Traumatic brain injury and grey matter concentration: a preliminary voxel based morphometry study. *Journal of Neurology, Neurosurgery, and Psychiatry*, *76*(7), 984–988. https://doi.org/10.1136/jnnp.2004.036210

Gentry, L. R., Godersky, J. C., & Thompson, B. (1988). MR imaging of head trauma: review of the distribution and radiopathologic features of traumatic lesions. *AJR. American Journal of Roentgenology*, *150*(3), 663–672. https://doi.org/10.2214/ajr.150.3.663

Gooijers, J., Beets, I. A. M., Albouy, G., Beeckmans, K., Michiels, K., Sunaert, S., & Swinnen, S. P. (2016). Movement preparation and execution: differential functional activation patterns after traumatic brain injury. *Brain*, *139*(9), 2469–2485. https://doi.org/10.1093/brain/aww177

Guskiewicz, K. M., Riemann, B. L., Perrin, D. H., & Nashner, L. M. (1997). Alternative approaches to the assessment of mild head injury in athletes. *Medicine and Science in Sports and Exercise*, *29*(7 Suppl), S213-221.

Ham, T. E., & Sharp, D. J. (2012). How can investigation of network function inform rehabilitation after traumatic brain injury? *Current Opinion in Neurology*, *25*(6), 662–669. https://doi.org/10.1097/WCO.0b013e328359488f

Hikosaka, O., & Isoda, M. (2010). Switching from automatic to controlled behavior: cortico-basal ganglia mechanisms. *Trends in Cognitive Sciences*, *14*(4), 154–161. https://doi.org/10.1016/j.tics.2010.01.006

Hillary, F. G., Genova, H. M., Chiaravalloti, N. D., Rypma, B., & DeLuca, J. (2006). Prefrontal modulation of working memory performance in brain injury and disease. *Human Brain Mapping*, *27*(11), 837–847. https://doi.org/10.1002/hbm.20226

Hillary, F. G., Slocomb, J., Hills, E. C., Fitzpatrick, N. M., Medaglia, J. D., Wang, J., … Wylie, G. R. (2011). Changes in resting connectivity during recovery from severe traumatic brain injury. *International Journal of Psychophysiology: Official Journal of the International Organization of Psychophysiology*, *82*(1), 115–123. https://doi.org/10.1016/j.ijpsycho.2011.03.011

Hulkower, M. B., Poliak, D. B., Rosenbaum, S. B., Zimmerman, M. E., & Lipton, M. L. (2013). A decade of DTI in traumatic brain injury: 10 years and 100 articles later. *AJNR. American Journal of Neuroradiology*, *34*(11), 2064–2074. https://doi.org/10.3174/ajnr.A3395

Katz-Leurer, M., Rotem, H., Lewitus, H., Keren, O., & Meyer, S. (2008). Relationship between balance abilities and gait characteristics in children with post-traumatic brain injury. *Brain Injury*, *22*(2), 153–159. https://doi.org/10.1080/02699050801895399

Kim, J., Parker, D., Whyte, J., Hart, T., Pluta, J., Ingalhalikar, M., … Verma, R. (2014). Disrupted structural connectome is associated with both psychometric and real-world neuropsychological impairment in diffuse traumatic brain injury. *Journal of the International Neuropsychological Society: JINS*, *20*(9), 887–896. https://doi.org/10.1017/S1355617714000812

Lancaster, J. L., Woldorff, M. G., Parsons, L. M., Liotti, M., Freitas, C. S., Rainey, L., … Fox, P. T. (2000). Automated Talairach atlas labels for functional brain mapping. *Human Brain Mapping*, *10*(3), 120–131.

Leunissen, I., Coxon, J. P., Caeyenberghs, K., Michiels, K., Sunaert, S., & Swinnen, S. P. (2014a). Subcortical volume analysis in traumatic brain injury: the importance of the fronto-striato-thalamic circuit in task switching. *Cortex; a Journal Devoted to the Study of the Nervous System and Behavior*, *51*, 67–81. https://doi.org/10.1016/j.cortex.2013.10.009

Leunissen, I., Coxon, J. P., Caeyenberghs, K., Michiels, K., Sunaert, S., & Swinnen, S. P. (2014b). Task switching in traumatic brain injury relates to cortico-subcortical integrity. *Human Brain Mapping*, *35*(5), 2459–2469. https://doi.org/10.1002/hbm.22341

Mäki-Marttunen, V., Diez, I., Cortes, J. M., Chialvo, D. R., & Villarreal, M. (2013). Disruption of transfer entropy and inter-hemispheric brain functional connectivity in patients with disorder of consciousness. *Frontiers in Neuroinformatics*, *7*, 24. https://doi.org/10.3389/fninf.2013.00024

Marinazzo, D., Pellicoro, M., Wu, G., Angelini, L., Cortés, J. M., & Stramaglia, S. (2014). Information transfer and criticality in the Ising model on the human connectome. *PloS One*, *9*(4), e93616. https://doi.org/10.1371/journal.pone.0093616

Mayer, A. R., Mannell, M. V., Ling, J., Gasparovic, C., & Yeo, R. A. (2011). Functional connectivity in mild traumatic brain injury. *Human Brain Mapping*, *32*(11), 1825–1835. https://doi.org/10.1002/hbm.21151

McCulloch, K. L., Buxton, E., Hackney, J., & Lowers, S. (2010). Balance, attention, and dual-task performance during walking after brain injury: associations with falls history. *The Journal of Head Trauma Rehabilitation*, *25*(3), 155–163. https://doi.org/10.1097/HTR.0b013e3181dc82e7

Mink, J. W. (1996). The basal ganglia: focused selection and inhibition of competing motor programs. *Progress in Neurobiology*, *50*(4), 381–425.

Mori, S., Crain, B. J., Chacko, V. P., & van Zijl, P. C. (1999). Three-dimensional tracking of axonal projections in the brain by magnetic resonance imaging. *Annals of Neurology*, *45*(2), 265–269.

Murphy, K., Birn, R. M., Handwerker, D. A., Jones, T. B., & Bandettini, P. A. (2009). The impact of global signal regression on resting state correlations: Are anti-correlated networks introduced? *NeuroImage*, *44*(3), 893–905. https://doi.org/10.1016/j.neuroimage.2008.09.036

Newman, M. E. J. (2004). Fast algorithm for detecting community structure in networks. *Physical Review E*, *69*(6). https://doi.org/10.1103/PhysRevE.69.066133

Palacios, E. M., Sala-Llonch, R., Junque, C., Roig, T., Tormos, J. M., Bargallo, N., & Vendrell, P. (2013). Resting-state functional magnetic resonance imaging activity and connectivity and cognitive outcome in traumatic brain injury. *JAMA Neurology*, *70*(7), 845–851. https://doi.org/10.1001/jamaneurol.2013.38

Park, H.-J., & Friston, K. (2013). Structural and Functional Brain Networks: From Connections to Cognition. *Science*, *342*(6158), 1238411–1238411. https://doi.org/10.1126/science.1238411

Rasmussen, I.-A., Xu, J., Antonsen, I. K., Brunner, J., Skandsen, T., Axelson, D. E., … Håberg, A. (2008). Simple Dual Tasking Recruits Prefrontal Cortices in Chronic Severe Traumatic Brain Injury Patients, But Not in Controls. *Journal of Neurotrauma*, *25*(9), 1057–1070. https://doi.org/10.1089/neu.2008.0520

Saad, Z. S., Gotts, S. J., Murphy, K., Chen, G., Jo, H. J., Martin, A., & Cox, R. W. (2012). Trouble at Rest: How Correlation Patterns and Group Differences Become Distorted After Global Signal Regression. *Brain Connectivity*, *2*(1), 25–32. https://doi.org/10.1089/brain.2012.0080

Sharp, D. J., Beckmann, C. F., Greenwood, R., Kinnunen, K. M., Bonnelle, V., De Boissezon, X., … Leech, R. (2011). Default mode network functional and structural connectivity after traumatic brain injury. *Brain: A Journal of Neurology*, *134*(Pt 8), 2233–2247. https://doi.org/10.1093/brain/awr175

Sharp, D. J., Scott, G., & Leech, R. (2014). Network dysfunction after traumatic brain injury. *Nature Reviews. Neurology*, *10*(3), 156–166. https://doi.org/10.1038/nrneurol.2014.15

Smith, D. H., & Meaney, D. F. (2000). Axonal Damage in Traumatic Brain Injury. *The Neuroscientist*, *6*(6), 483–495. https://doi.org/10.1177/107385840000600611

Smith, S. M., Fox, P. T., Miller, K. L., Glahn, D. C., Fox, P. M., Mackay, C. E., … Beckmann, C. F. (2009). Correspondence of the brain's functional architecture during activation and rest. *Proceedings of the National Academy of Sciences of the United States of America*, *106*(31), 13040–13045. https://doi.org/10.1073/pnas.0905267106

Squarcina, L., Bertoldo, A., Ham, T. E., Heckemann, R., & Sharp, D. J. (2012). A robust method for investigating thalamic white matter tracts after traumatic brain injury. *NeuroImage*, *63*(2), 779–788. https://doi.org/10.1016/j.neuroimage.2012.07.016

Stramaglia, S., Angelini, L., Cortes, J. M., & Marinazzo, D. (2015). Synergy, redundancy and unnormalized Granger causality. *Conference Proceedings: ... Annual International Conference of the IEEE Engineering in Medicine and Biology Society. IEEE Engineering in Medicine and Biology Society. Annual Conference*, *2015*, 4037–4040. https://doi.org/10.1109/EMBC.2015.7319280

Stramaglia, S., Angelini, L., Wu, G., Cortes, J. M., Faes, L., & Marinazzo, D. (2016). Synergetic and redundant information flow detected by unnormalized Granger

causality: application to resting state fMRI. *IEEE Transactions on Biomedical Engineering*, 1–1. https://doi.org/10.1109/TBME.2016.2559578

Tagliazucchi, E., Balenzuela, P., Fraiman, D., & Chialvo, D. R. (2012). Criticality in Large-Scale Brain fMRI Dynamics Unveiled by a Novel Point Process Analysis. *Frontiers in Physiology*, *3*. https://doi.org/10.3389/fphys.2012.00015

Tarapore, P. E., Findlay, A. M., Lahue, S. C., Lee, H., Honma, S. M., Mizuiri, D., … Mukherjee, P. (2013). Resting state magnetoencephalography functional connectivity in traumatic brain injury. *Journal of Neurosurgery*, *118*(6), 1306–1316. https://doi.org/10.3171/2013.3.JNS12398

Tzourio-Mazoyer, N., Landeau, B., Papathanassiou, D., Crivello, F., Etard, O., Delcroix, N., … Joliot, M. (2002). Automated anatomical labeling of activations in SPM using a macroscopic anatomical parcellation of the MNI MRI single-subject brain. *NeuroImage*, *15*(1), 273–289. https://doi.org/10.1006/nimg.2001.0978

Van Impe, A., Coxon, J. P., Goble, D. J., Doumas, M., & Swinnen, S. P. (2012). White matter fractional anisotropy predicts balance performance in older adults. *Neurobiology of Aging*, *33*(9), 1900–1912. https://doi.org/10.1016/j.neurobiolaging.2011.06.013

Wade, L. D., Canning, C. G., Fowler, V., Felmingham, K. L., & Baguley, I. J. (1997). Changes in postural sway and performance of functional tasks during rehabilitation after traumatic brain injury. *Archives of Physical Medicine and Rehabilitation*, *78*(10), 1107–1111.

Yan, C.-G., Cheung, B., Kelly, C., Colcombe, S., Craddock, R. C., Di Martino, A., … Milham, M. P. (2013). A comprehensive assessment of regional variation in the impact of head micromovements on functional connectomics. *NeuroImage*, *76*, 183–201. https://doi.org/10.1016/j.neuroimage.2013.03.004

Zalesky, A., Fornito, A., & Bullmore, E. T. (2010). Network-based statistic: Identifying differences in brain networks. *NeuroImage*, *53*(4), 1197–1207. https://doi.org/10.1016/j.neuroimage.2010.06.041

Zappalà, G., Thiebaut de Schotten, M., & Eslinger, P. J. (2012). Traumatic brain injury and the frontal lobes: what can we gain with diffusion tensor imaging? *Cortex; a Journal Devoted to the Study of the Nervous System and Behavior*, *48*(2), 156–165. https://doi.org/10.1016/j.cortex.2011.06.020

Zhou, Y., Milham, M. P., Lui, Y. W., Miles, L., Reaume, J., Sodickson, D. K., … Ge, Y. (2012). Default-mode network disruption in mild traumatic brain injury. *Radiology*, *265*(3), 882–892. https://doi.org/10.1148/radiol.12120748

<Figure Captions>

Figure 1: TBI-induced alterations to structural networks revealed by diffusion tensor imaging. a: Hierarchical tree or dendrogram defining the hierarchal brain partition (Diez, Bonifazi, et al., 2015) where three different levels of the tree have been emphasized: *M=1*, where all brain regions belong to a single module; *M=20*, the optimal brain partition (see Methods); and *M=120*, the level at which structural connectivity was higher in TBI than in the controls. Group differences were calculated on module degree maps calculated on the inter-module connectivity matrix and after a two sample t-test with age and head motion as covariate of non-interest ($p<0.05$). Multiple comparison corrections were achieved by applying subject label permutations, thereby building the null-hypothesis distribution as all correlations were removed by shuffling. Greater connectivity in controls than in TBI (red

scale) was found at *M=20*, whilst at *M=120*, TBI > control connectivity was also found (blue scale). Brain maps represent t-statistic values. **b:** At *M=20* (left graph), significant control > TBI connectivity was evident in module 14 (including part of the hippocampus and parahippocampal gyrus, amygdala, putamen, insula, ventral diencephalon, temporal gyrus and temporal pole) and module 20 (including part of the cerebellum and parahippocampal gyrus). At *M=120* (right graph), TBI > control connectivity was found within the module 11, including part of the rectus and the superior and inferior frontal orbital gyrus. Module colours are just indicative, and coincide with the colours published in (Diez, Bonifazi, et al., 2015), where we first published the brain hierarchical atlas.

Figure 2: TBI-induced alterations to brain dynamics within individual modules revealed by resting state fMRI. For each of the *M=20* modules in the hierarchical atlas, we extracted the time-series of the first principal component and calculated four different descriptors: the variance, skewness, kurtosis and number of points after the PPA (Methods). **a:** Only module 11 showed differences between the TBI and control with respect to the variance of the time series of the first principal component. The dashed lines represent the mean value of the time series and the solid lines represent the threshold used for the PPA, here equal to the mean + 1 SD. **b:** For module 11, the variance of the first component (plotted here as its square root, i.e.: the standard deviation) differed between TBI and control subjects. In particular, the fact that the variance was higher in TBI (red) as compared to control (blue) showed compensation rather than a deficit. Module 11 colour (magenta) is just indicative, and coincide with the colours published in (Diez, Bonifazi, et al., 2015), where we first published the brain hierarchical atlas.

Figure 3: Prefrontal recruitment into a subcortical network. Significant brain maps after using different contrasts: Column 1,"FN in control", with a red bar and corresponding to the contrast [1 0 0 0] (Methods); Column 2,"FN in TBI", with a blue bar and corresponding to the contrast [0 1 0 0]; Column 3, "differences" and corresponding to two contrasts, [1 -1 0 0] and [-1 1 0 0], represented in red (control > TBI activation) and blue (TBI > control activation), respectively. TBI patients (but not control participants) recruited the prefrontal part of the brain when interacting with a subcortical network (coloured in blue at the column "differences"). In all cases, the bar-scale represents the significance strength, measured by the t-statistic values. Contrasts [1 0 0 0] and [0 1 0 0] define the "subcortical network" (which corresponds to one MRC including part of the cerebellum, the basal ganglia, the thalamus, the amygdala and the temporal poles). This network resulted from the interactions coming from module 3 (including part of the sensory-motor and auditory networks), modules 14 and 15 (including part of the thalamus, hippocampus, amygdala, putamen, ventral diencephalon and insula); module 18 (including part of the hippocampus and entorhinal cortex, fusiform gyrus, inferior and middle temporal gyrus, and parahippocampal gyrus); module 19 (including part of the cerebellum and brainstem); and region 20 (including part of the cerebellum and parahippocampal gyrus). Module colours are just indicative, and coincide with the colours published in (Diez, Bonifazi, et al., 2015), where we first published the brain hierarchical atlas.

Figure 4: Prefrontal recruitment into the task-positive interactions. As in figure 3 but the MRC now resembles the task-positive network (see labels "FN in control" and "FN in

TBI"), which is now resulting from module 1 (posterior cingulate cortex); module 4 (medial visual cortex); region 5 (medial frontal gyrus); module 12 (inferior parietal and temporal gyrus, lateral frontal orbital gyrus, rostral pars of the middle frontal gyrus and pars orbitalis and triangularis); and modules 14 and 15 (subcortical structures). Similar to what it was shown in figure 3, now TBI patients recruited the prefrontal part of the brain when interacting to the task-positive network (coloured in blue at the column "differences").

Figure 5: Common regions where TBI > control connectivity resulted from both structural and functional network analyses. a: Structural network compensation. TBI > control structural connectivity occurred within a subnetwork consisting of a hub (coloured in red) connected to other regions (coloured in green); the hub includes the orbitofrontal and rectus regions and belongs to the module 11 in the *M=20* hierarchical atlas. The regions connected to the hub are frontal superior regions, the anterior cingulum, the thalamus, the striatum, the insula, the amygdala, the hippocampus and para-hippocampus, the olfactory cortex and the cerebellum. The corrected variance of the first principal component of module 11 was also correlated with postural control measures; here it is represented the iPL-SOT score. **b:** Functional network compensation. TBI > control functional connectivity (blue) occurred when interacting with subcortical structures (including the superior frontal gyrus, the superior medial frontal and the middle frontal gyri, and the anterior cingulum) and the task-positive network (including the anterior cingulum, the medial frontal and middle orbital gyri, the superior frontal medial gyrus and the rectus). For both situations, the spatial maps represent the functional the result of averaging all spatial maps with contrast [-1 1 0 0] in figure 3 (“subcortical network”) and figure 4 (“task-positive network”). Thus, TBI

patients (but not control participants) incorporated to both the subcortical and the task-positive networks the prefrontal brain of the brain.

<Tables>

Table 1: Demographic data of TBI patients. TA = Traffic Accident; C = Coma; NA = Information not available; GCS = Glasgow Coma Scale score; M = male; F = female

ID	Age	Gender (y)	Cause of injury	Age at injury (y)	Time since injury (y)	GCS/coma duration
T01	8.6	M	TA	7.9	0.7	C: 5 days
T02	18.1	F	TA	15.6	2.5	C: 5 days
T03	9.3	F	TA	7.9	1.4	C: 2 weeks
T04	16.5	F	TA	7.2	9.3	NA
T05	14.2	F	TA	7.7	6.5	NA
T06	13.4	M	TA	12.5	0.8	NA
T07	19.0	F	Fall	12.5	6.5	NA
T08	15.6	M	TA	12.5	3.2	C: 10 days
T09	13.9	M	TA	13.5	0.3	GCS: 3
T10	8.5	F	TA	7.7	0.8	NA
T11	11.4	M	Sports injury	9.8	1.5	NA
T12	13.3	M	TA	12.1	1.2	NA
T13	16.0	F	NA	NA	NA	NA
T14	13.8	F	Object	3.0	10.8	NA

Diez, Ibai, et al. (2017) Enhanced pre-frontal functional-structural networks to support postural control deficits after traumatic brain injury in a pediatric population. *Network Neuroscience*. Advance online publication. doi:10.1162/netn_a_00007.

Impact

Diez, Ibai, et al. (2017) Enhanced pre-frontal functional-structural networks to support postural control deficits after traumatic brain injury in a pediatric population. *Network Neuroscience*. Advance online publication. doi:10.1162/netn_a_00007.

Table 2: Clinical data of TBI patients.

ID	Acute MRI scan within 24 h after injury lesion location/pathology	MRI scan analyzed in this study lesion location/pathology
T01	Subdural hematoma R FL/PL/TL; cortical contusion R FL/PL; DAI in R FL	Hemosiderin deposits: R semiovale centre and CC
T02	Subdural hematoma/hemorrhagic contusion TL/FL; injuries R FL, thalamus, R cerebral peduncle, L mesencephalon; cortical and subcortical hemorrhagic areas in PL/TL	Small injuries surrounding drain trajectory in RH (superior frontal gyrus, head nucleus caudatus, crus anterius of internal capsule, thalamus, and pons)
T03	DAI in L TL/FL, R TL/FL/PL	Contusion: R anterior temporal pole and R orbitofrontal cortex; Injuries and atrophy in CC (body and splenium); Atrophy of R pons; Hemosiderin deposits in L cerebellar hemisphere, R nucleus lentiformis, L/R FL, L/R PL and R PL
T04	Epidural hematoma R FL/TL; shift midline	Injuries in R medial frontal gyrus.
T05	NA	Atrophy of the cerebellum; Injuries at the level of L

		FL, premotor cortex, L/R medial frontal gyrus, cingulum, orbitofrontal cortex (L>R); Contusion anterior temporal pole (R>L); Hemosiderin deposits in CC, L thalamus, striatum (R>L)
T06	Hemorrhagic contusion L TL; brain oedema	Hemosiderin deposits: several spread out over L/R PL, R cerebellum, L superior frontal gyrus. Hemociderosis as a remnant of subdural hemorrhage
T07	Subdural hematoma L FL/TL/PL	Hemosiderin deposits R cerebellar vermis
T08	DAI R TL, internal capsule, supra-orbital R FL, L FL WM (anterior corona radiata), L middle cerebellar peduncle	Atrophy cerebellum; Contusion R FL WM
T09	DAI FL, TL, L OL (hemorrhagic injury), cerebellum, CC, external capsule, R globus pallidus, L thalamus, R cerebral peduncle, R mesencephalon	Hemosiderin deposits: L FL, periventricular WM, body and genu CC, L thalamus, R external capsule, anterior TL (L>R), L/R cerebellum; limited atrophy cerebellum
T10	NA	Enlarged fourth ventricle, atrophy of cerebellar vermis, contusion R cerebellar vermis, hypotrophy of middle cerebellar peduncle and L pons; contusion L TL; Hemosiderin deposits R FL, L TL, Vermis

T11	Contusion L FL/TL; Enlarged, asymmetric ventricle (temporal horn)	Hemosiderin deposit: splenium CC
T12	DAI in genu and splenium CC, L FL	Hemosiderin deposits L FL, genu CC
T13	NA	Mild atrophy in cerebellum and cerebrum, more pronounced atrophy in frontal cortices, enlarged ventricles; contusion L/R anterior temporal pole and L/R orbitofrontal cortex. Hemosiderin deposits in cerebellum, R FL
T14	Hemorrhagic contusion L FL, atrophy L FL	Contusion: L anterior middle frontal gyrus and L anterior superior frontal gyrus

*WM=white matter; RH=right hemisphere; LH=left hemisphere; FL=frontal lobe; TL=temporal lobe; PL=parietal lobe; OL=occipital lobe; CC=corpus callosum; R = right; L = left.

Diez, Ibai, et al. (2017) Enhanced pre-frontal functional-structural networks to support postural control deficits after traumatic brain injury in a pediatric population. *Network Neuroscience*. Advance online publication. doi:10.1162/netn_a_00007.

Table 3: Anatomical description of the *M=20* modules in the hierarchical atlas published recently (Diez, Bonifazi, et al., 2015) **and available to download at** http://www.nitrc.org/projects/biocr_hcatlas/ **.** In the first column, we also indicate module volumes.

Module (volume size)	**Anatomical description**
Module 1 (7.26 cm^3)	**Posterior cingulate:** posterior area of the cingulate gyrus or callosal convolution. Located above the corpus callosum, it goes from the frontal lobe back to the temporal uncus and up to the splenium. It belongs to the Default Mode Network.
Module 2 (104.36 cm^3)	**Putamen:** a round structure located at the base of the telencephalon. It is also one of the basal ganglia structures. **Anterior cingulate:** anterior frontal region of the cingulate gyrus, initiated above the rostrum of the corpus callosum. **Rostral pars of the middle frontal gyrus:** anterior inferior end of the middle frontal gyrus. **Superior parietal gyrus:** parietal gyrus located posterior to the postcentral gyrus. **Supramarginal gyrus**: region in the parietal lobe encircling the posterior extreme of the Sylvian fissure. **Insula:** triangular area of cerebral cortex forming the medial wall of the Sylvian fissure. **Inferior parietal gyrus:** parietal gyrus located behind the postcentral gyrus and below the superior parietal gyrus. **Precentral gyrus:** frontal gyrus that defines the anterior boundary of the fissure of Rolando with a mainly motor function. **Superior frontal gyrus:** antero-superior parasagittal frontal gyrus, located anterior to the precentral gyrus.
Module 3 (221.18 cm^3)	**Paracentral lobule:** medial gyrus that connects the pre- and postcentral gyrus. **Precentral gyrus** (cf. region 2) **Postcentral gyrus:** Parietal gyrus located between the fissure of Rolando and the postcentral

	sulcus, which has a mainly sensory function. **Precuneus:** square brain lobule located before the parietal-occipital sulcus and behind the paracentral lobule at the medial surface of the brain hemisphere. **Superior frontal gyrus** (cf. region 2). **Superior parietal gyrus** (cf. region 2) **Superior temporal gyrus:** temporal gyrus at the lateral surface of the temporal lobe. It is located below the Sylvian fissure and above the superior temporal sulcus. It belongs to the temporal neocortex. **Supramarginal gyrus** (cf. region 2). **Insula** (cf. region 2)
Module 4 (91.48 cm^3)	**Cuneus:** occipital gyrus between the parieto-occipital sulcus and the calcarine sulcus at the medial surface of the occipital lobe. **Lateral occipital sulcus:** external lateral surface of the occipital lobe close to the occipital lobe, dividing the external occipital gyrus. **Lingual gyrus:** occipital extension of the parahippocampal gyrus at the medial surface of the occipital lobe. **Pericalcarine cortex:** occipital area encircling the calcarine sulcus with a function associated to visual perception. **Precuneus** (cf. region 3)
Module 5 (37.02 cm^3)	**Medial frontal gyrus:** frontal gyrus at the lateral surface below the superior frontal gyrus. **Precentral gyrus** (cf. region 2) **Rostral pars of the middle frontal gyrus** (cf. region 2)
Module 6 (159.33 cm^3)	**Cerebellum:** posterior part of the rombencephalon made up of the two hemispheres and the central vermis. It is located below the occipital lobe. **Fusiform gyrus:** temporal gyrus in the inferior surface between the inferior temporal gyrus and the parahippocampal gyrus. It has two areas, the medial occipito-temporal gyrus and the lateral occipito-temporal gyrus. **Inferior temporal gyrus:** inferior gyrus located in the lateral surface of the temporal lobe, below the inferior temporal sulcus.

	Lateral occipital sulcus (cf. region 4) **Superior parietal gyrus** (cf. region 2)
Module 7 (22.30 cm^3)	**Thalamus:** middle symmetrical structure of the diencephalon with multiple afferent and efferent connections, situated around the third ventricle. **Caudate nucleus** (symmetrical structure): one of the basic structures of the basal ganglia belonging to the corpus striatum. It is located at the lateral surface of the lateral ventricles surrounding the thalamus. **Putamen** (cf. region 2) **Pallidum:** symmetrical structure within the basal ganglia. Medial diencephalic region of the lenticular nucleus. **Accumbens nucleus:** symmetrical structure located in the ventral region of the corpus striatum, therefore belonging to the basal ganglia.
Module 8 (3.29 cm^3)	**Caudate nucleus** (cf. region 7) **Putamen** (cf. region 2)
Module 9 (163.67 cm^3)	**Cerebellum** (cf. region 6) **Caudal middle frontal:** frontal gyrus on the lateral surface located below and lateral to the superior frontal gyrus. This region refers to its most caudal part. **Cingulate isthmus:** intersection narrowing between the cingulate and the hippocampal gyrus. It is located behind and below the splenium of the corpus callosum. **Posterior cingulate** (cf. region 1) **Precuneus** (cf. region 3) **Inferior parietal gyrus** (cf. region 2) **Rostral pars of the middle frontal gyrus** (cf. region 2) **Superior frontal gyrus** (cf. region 2)
Module 10 (103.55 cm^3)	**Anterior cingulate** (cf. region 2) **Inferior parietal gyrus** (cf. region 2) **Orbital gyrus:** frontobasal gyrus lateral located to the straight gyrus. **Pars opercularis:** opercular part of the inferior frontal gyrus. **Pars orbitalis:** orbital part of the inferior frontal gyrus.

	Pars triangularis: inferior part of the inferior frontal gyrus. **Anterior cingulate** (cf. region 2) **Rostral pars of middle frontal gyrus** (cf. region 2) **Superior frontal gyrus** (cf. region 2)
Module 11 (31.08 cm^3)	**Caudate nucleus** (cf. region 7) **Accumbens nucleus** (cf. region 7) **Lateral frontal orbital gyrus:** external orbital gyrus, located frontobasal and lateral to the medial orbitofrontal gyrus. **Orbital gyrus** (cf. region 10) **Anterior cingulate** (cf. region 10)
Module 12 (33.24 cm^3)	**Inferior parietal gyrus** (cf. region 2) **Inferior temporal gyrus** (cf. region 6) **Lateral frontal orbital gyrus** (cf. region 11) **Pars orbitalis** (cf. region 10) **Pars triangularis** (cf. region 10) **Rostral pars of the middle frontal gyrus** (cf. region 2) **Superior frontal gyrus** (cf. region 2) **Caudate nucleus and anterior cingulate** (cf. region 7 and region 2)
Module 13 (24.46 cm^3)	**Middle frontal gyrus:** caudal part of the middle frontal gyrus. **Pars opercularis** (cf. region 10) **Precentral gyrus** (cf. region 2) **Superior frontal gyrus** (cf. region 2)
Module 14 (92.75 cm^3)	**Thalamus** (cf. region 7) **Hippocampus:** symmetrical grey matter structure, located in the mesial-temporal region, at the base of the temporal horn. **Amygdala:** grey nuclei located in the temporal uncus, above the temporal ventricular horn. It belongs to the rhinencephalon. **Putamen** (cf. region 2) **Ventral diencephalon:** multiple structures containing the hypothalamus, mammillary tubercle,

	subthalamic nucleus, substantia nigra, red nucleus, geniculate body, optic tract and cerebral peduncles. **Banks of the superior temporal sulcus:** Temporal lobe structure between the superior temporal gyrus and the middle temporal gyrus. **Parahippocampal gyrus:** convolution located below the hippocampal sulcus in the temporal mesial region. **Superior temporal gyrus** (cf. region 3) **Insula** (cf. region 2) **Middle temporal gyrus:** gyrus located on the lateral surface of the temporal lobe between the inferior and superior temporal sulcus. **Temporal pole:** anterior end of the temporal lobe.
Module 15 (42.96 cm^3)	**Thalamus** (cf. region 7) **Putamen** (cf. region 2) **Pallidum** (cf. region 7) **Brainstem:** it consists of three parts, the myelencephalon, pons (metencephalon) and midbrain (mesencephalon). It is the main communication route between the brain, spinal cord and peripheral nerves. **Hippocampus** (cf. region14) **Amygdala** (cf. region 14) **Accumbens nucleus** (cf. region 7) **Ventral diencephalon** (cf. region 14) **Orbital gyrus** (cf. region 10) **Insula** (cf. region 2)
Module 16 (65.58 cm^3)	**Cerebellum** (cf. region 6) **Banks of the superior temporal sulcus** (cf. region 14) **Inferior parietal gyrus** (cf. region 2) **Cingulate isthmus** (cf. region 9) **Middle temporal gyrus** (cf. region 14) **Precuneus** (cf. region 3)

	Superior temporal gyrus (cf. region 3)
Module 17 (5.29 cm^3)	**Banks of the superior temporal sulcus** (cf. region 14) **Middle temporal gyrus** (cf. region 14)
Module 18 (74.39 cm^3)	**Hippocampus** (cf. region 14) **Amygdala** (cf. region 14) **Entorhinal cortex**: area in the medial-temporal lobe located between the hippocampus and temporal neocortex. **Fusiform gyrus** (cf. region 6) **Inferior temporal gyrus** (cf. region 6) **Middle temporal gyrus** (cf. region 14) **Parahippocampal gyrus** (cf. region 14) **Temporal pole** (cf. region 14)
Module 19 (28.54 cm^3)	**Cerebellum** (cf. region 6) **Brainstem** (cf. region 15)
Module 20 (34.91 cm^3)	**Cerebellum** (cf. region 6) **Parahippocampal gyrus** (cf. region 14)

Table 4: TBI vs control differences with respect to structural networks revealed by diffusion tensor imaging (cf. figure 1).

At the level of *M=20* modules				
Module	*t-statistic*	*p-value*	*Effect size (Hedges)*	*Confidence intervals*
14	2.6351	0.0120	0.8511	0.1539 0.2990
20	3.1276	0.0033	1.0101	1.5152 1.6821

At the level of *M=120* regions					
Module120	*Module20*	*t-statistic*	*p-value*	*Effect size (Hedges)*	*Confidence intervals*
1	11	-2.7511	0.0090	-0.8885	-1.5544 -0.1883
25	12	2.6874	0.0105	0.8679	0.1694 1.5329
45	13	2.2003	0.0338	0.7106	0.0244 1.3694
70	6	2.6289	0.0122	0.8491	0.1521 1.5131
72	6	2.4432	0.0192	0.7891	0.0969 1.4507
79	14	2.2327	0.0314	0.7211	0.0341 1.3802
84	14	2.7039	0.0101	0.8733	0.1743 1.5384
85	14	2.4728	0.0179	0.7986	0.1057 1.4606
87	14	2.8865	0.0063	0.9323	0.2282 1.6002
88	14	3.4186	0.0015	1.1041	0.3840 1.7815
106	18	2.4281	0.0199	0.7842	0.0924 1.4456
114	19	2.7931	0.0080	0.9021	0.2007 1.5686
117	20	3.3141	0.0020	1.0703	0.3535 1.7457
118	20	2.5526	0.0147	0.8244	0.1295 1.4874

119	20	2.2096	0.0331	0.7136	0.0272 1.3725

Table 5: TBI vs control differences with respect to brain dynamics within individual modules revealed by resting state fMRI (cf. figure 2)

Module	*t-statistic*	*p-value*	*Effect size (Hedges)*	*confidence intervals*
11 (variance)	-2.5512	0.0148	-0.8240	-1.4870 -0.2000

Diez, Ibai, et al. (2017) Enhanced pre-frontal functional-structural networks to support postural control deficits after traumatic brain injury in a pediatric population. *Network Neuroscience*. Advance online publication. doi:10.1162/netn_a_00007.

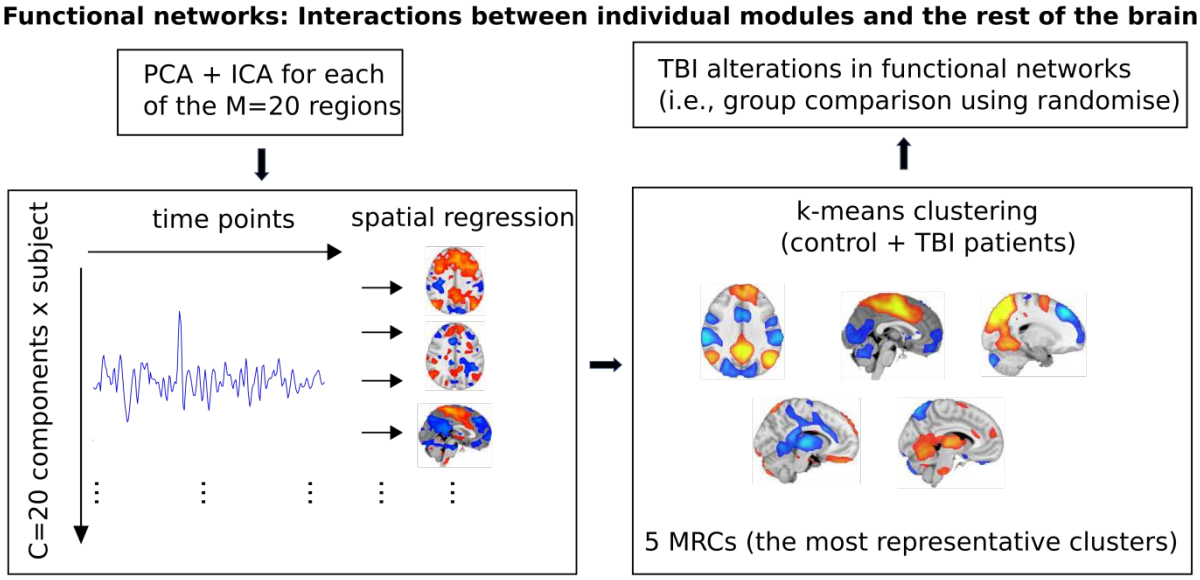

Figure S1: Sketch for the method to obtain functional interactions between individual modules and the rest of the brain. The alterations to the interaction network induced by TBI were addressed by applying a PCA+ICA to each of the *M=20* modules in order to extract *C=20* components for each module. These components were then spatially regressed to all the brain's voxels in order to identify which voxels outside the region interacted most with each component (i.e.: to obtain the spatial map for each component). Finally, all the spatial maps were clustered using k-means, which provided the 5 MRCs (most representative clusters) that correspond to the 5 main networks that each of the *M=20* modules interact with.